OPTIMAL WING ASPECT RATIO OF HIGHLY EFFICIENT LONG-RANGE AIRCRAFT

Tobias Franziskus Wunderlich [1]

[1]German Aerospace Center (DLR), Institute of Aerodynamics and Flow Technology,
Lilienthalplatz 7, 38108 Braunschweig, Germany

Abstract

This work investigates the potential of higher aspect ratio wings to improve the fuel efficiency of long-range aircraft. The main characteristics of high aspect ratio wings are briefly discussed and a process for aero-structural wing optimization is presented.
Adaptive wing technologies based on trailing edge control surface deflections to achieve optimal lift distributions to minimize drag in cruise flight and maximize load reduction in maneuver flight are considered and supplemented by advanced structural technologies with increased strain allowable and post-buckling to reduce wing mass. In the optimization process, high-fidelity simulation methods are used to determine the flight performance in transonic cruise flight, the loads on the wing in maneuver flight and the mass of the composite wing box. Static aeroelastic effects are taken into account in all flight conditions. The minimization of fuel consumption for three typical flight missions represents the objective function. The geometric integration of the control surfaces and aircraft trim are taken into account.
The application of the process to optimize the wing planform, twist distribution and the control surface deflections forms the main part of this publication. The results show an optimal wing aspect ratio in the order of 12. A further increase in aspect ratio to a value of 13.5 shows no further improvement in aerodynamic performance and the resulting fuel consumption.

Keywords: high aspect ratio wing, adaptive wing, multidisciplinary design optimization, aircraft design

1. Introduction

The environmental impact and resource requirements of commercial aviation are increasing with the growth of global mobility and transportation. To protect the environment and conserve resources, aviation is undergoing a transformation process toward more energy-efficient air transport. DLR's Aviation Research Strategy [1] describes and specifies the contribution of aeronautics research to achieving the goals of the mobility strategy of the European Green Deal [2]. The corresponding target for the vehicle is a $25\,\%$ reduction in specific engine fuel consumption and a $50\,\%$ reduction in the aircraft's energy requirements.
The efficiency of commercial aircraft is determined by aerodynamic performance in terms of the lift-to-drag ratio, the empty mass of the aircraft and the thrust-specific fuel consumption of the engine. An aerodynamically optimized shape can further reduce drag in transonic cruise flight. This is achieved through advances in wing and airfoil design. Composite materials such as carbon fiber-reinforced polymers (CFRP) allow adapting the structural design to the loads by exploiting the additional degree of freedom of fiber orientation. Geared turbofan technology promises to further reduce thrust-specific fuel consumption by increasing propulsion efficiency.
Fundamental work on multidisciplinary wing design was published by Prandtl [3] and Jones [4]. In these works, the lift distribution with minimum induced drag is determined by specifying the lift coefficient and bending moment. Prandtl uses the integrated bending moment and Jones the root bending moment as a constraint. In the publication by Pate and German [5], the results of these works were generalized, which allows a minimization of the induced drag for the lift coefficient in cruise flight under

consideration of several constraints of the bending moment for different lift coefficients in maneuver flight.
In overall aircraft design, for example, Krengel [6] developed a method that additionally includes structural sizing of the wing box, taking into account the aeroelastic wing deformations and structural dynamics in the wing planform optimization. Based on this methodology, multidisciplinary wing optimizations were performed to investigate the potential of load reduction to minimize fuel consumption. The result is an optimal wing aspect ratio in the order of 12.
Advanced structural technologies and the adaptive wing are enablers for higher aspect ratio wings with improved aerodynamic performance.
In the design process of composite structures a damaged tolerance design allowable typically limits the permitted strain level. The dependency of the damage tolerance allowable from the ply share of the laminate was investigated by Bogenfeld et al. [7]. Based on the results of these studies an allowable increase between $30\,\%$ and $50\,\%$ was identified. The introduction of new structural concepts in terms of load share between skin and stiffeners (e.g. “stringer dominant design”) and ply share selection an increased strain allowable results in mass reduction of the wing box. Further mass reduction potential was identified due to permit local buckling after limit load (“post-buckling”). In addition, the increased allowables lead to more flexible wing structures that increase passive load alleviation.
Further improvements can be achieved by adapting the wing shape to the current flight condition. Adaptive wing technology has long been researched by industry and academia and has been summarized, for example, by Martins [8] under the synonym of morphing wing. For practical implementation, variable camber using trailing edge devices is the most promising type of wing morphing. The basic phenomena of variable camber, the corresponding wing design philosophy and system requirements, and the advantages of the new wing concept are described by Szodruch and Hilbig [9]. Aero-structural design optimization published by Burdette, Kenway, and Martins [10] shows a potential $1.7\,\%$ reduction in fuel consumption by using a $10\,\%$ deep continuous morphing trailing edge. Reckzeh [11] describes the wing movables concept of the Airbus A350 in service. This concept provides a functional integration of high-lift with load and cruise performance control. The potential for reducing fuel consumption by improving cruise performance was investigated for a long-range passenger aircraft in our own research [12]. Depending on the flight mission a fuel burn reduction between $0.5\,\%$ and $1.7\,\%$ was predicted.
In the context of aero-structural wing optimization, the optimal trade-off between cruise performance and wing mass is achieved by combining high-fidelity methods for numerical flow simulation of the aircraft outer shape and the structural sizing of the wing box with an appropriate optimization algorithm [13]. Thereby, the interaction of aerodynamic forces and wing deformations are considered to enable accurate prediction of flight performance and static maneuver loads using fluid-structure coupling.

2. Characteristics of High Aspect Ratio Wings

In this section the characteristics of high aspect ratio wings are described to show the potential, interactions and limitations of increasing the wingspan.

2.1 Induced Drag Reduction

The reason for increasing the aspect ratio is the potential to reduce induced drag. According to Munk’s stagger theorem [14], the induced drag for planar wings is only dependent on the lift distribution in the spanwise direction. This means that the induced drag for planar wings can be calculated from the lift distribution using the equations of simple lifting line theory [15]. The induced drag coefficient can be determined according to the simple lifting line theory using the well-known equation 1.

$$C_{Di} = \frac{C_L^2}{\pi\, e\, A_W} \tag{1}$$

Accordingly, the induced drag coefficient C_{Di} depends on the lift coefficient C_L, the wing aspect ratio A_W and the Oswald’s efficiency factor e. The shape of the lift distribution is taken into account by the Oswald’s efficiency factor, which has values less than or equal to one. The minimum induced

drag coefficient of planar wings is achieved with an elliptical lift distribution with an Oswald's efficiency factor of one.
The center of lift η_{CoL} significantly influences the wing mass and should have the lowest possible values with regard to a low wing mass. From an aerodynamic point of view, it is important to use the lift distribution with minimum induced drag for a given value of the center lift according to Equation 2.

$$e_{min\,CDi} = \frac{1}{\frac{9}{2}\,\pi^2\,\eta_{CoL}^2 - 12\,\pi\,\eta_{CoL} + 9.15} \tag{2}$$

This equation was first published by Jones [4] and modified here to take into account the lift drop in the fuselage region of classic tube and wing configurations (factor 9.0 has been replaced by 9.15).
The potential for reducing induced drag has been estimated using handbook methods from overall aircraft design using the Equations 1 and 2 for long-range aircraft with fixed wing loading of $m_{MTO}/S_W = 650\,\mathrm{kg\,m^{-2}}$ and has been summarized in Table 1.

Aspect ratio	A_W	**Baseline wing** 10.28 -	**Higher aspect ratio wing** 11.80 +14.8 %		**Ultra-high aspect ratio wing** 13.50 +31.3 %	
Center of lift	η_{CoL}	0.3850	0.3850	0.3600	0.3850	0.3350
	y_{CoL}	22.7 m	24.3 m	22.8 m	26.0 m	22.6 m
Oswald's efficiency factor	$e_{min\,CDi}$	0.820	0.820	0.749	0.820	0.664
Lift coefficient	$C_{L,max\,L/D}$	0.50	0.51	0.50	0.51	0.50
Induced drag coefficient	C_{Di}	0.0092	0.0084	0.0090	0.0076	0.0089
Drag coefficient	C_D	0.0264	0.0255	0.0260	0.0247	0.0258
Induced drag to drag ratio	C_{Di}/C_D	35.1 %	32.9 %	34.5 %	30.7 %	34.5 %
Lift-to-drag ratio	L/D	18.78 -	19.81 +5.4 %	19.21 +2.3 %	20.78 +10.6 %	19.40 +3.3 %

Table 1 – Estimated influence of aspect ratio to lift-to-drag ratio under cruise flight conditions.

The considered wing aspect ratios correspond to the wings presented in Section 3.4. For wings with the increased aspect ratio, a variant with a constant relative position of the center of lift and a variant with a constant absolute position of the center of lift have been calculated. A constant value of the absolute position of the center of lift corresponds to comparable aerodynamic loads under cruise flight conditions, which depend on the bending stiffness of the wing in connection with the dimensioning loads in maneuvering flight. The Oswald's efficiency factor calculated with the Equation 2 leads to minimum induced drag for the given position of the center of lift. With the lift coefficient for maximum lift-to-drag ratio given in Table 1 and the resulting induced drag, the corresponding improvements for the lift-to-drag ratio are obtained. For long-range aircraft, the improvements achieved are limited due to the relatively low drag component of the induced drag. With a similar level of aerodynamic loads in cruise flight compared to the baseline wing (modeled here with constant center of lift), the possible improvement of the lift-to-drag ratio by increasing the aspect ratio are in the order of $2\,\%$ for an aspect ratio increased by $15\,\%$ and in the order of $3\,\%$ for an aspect ratio increased by $30\,\%$. In combination with a shift of the center of lift towards the outer wing (constant relative center of lift is assumed here), an improvement of the lift-to-drag ratio in the order of $10\,\%$ can be expected for an increase in aspect ratio of $30\,\%$.

2.2 Geometric Constraints

For reasons of conformity with airport infrastructure, commercial aircraft are divided into FAA groups and ICAO codes. For each FAA group and ICAO code there is a limitation on the wingspan. One way to overcome this wingspan limitation is to use a folding wing tip to comply with the wingspan limitation on the parking position.
Further geometric constraints result from the integration of the main landing gear, the engine and the control surfaces as shown in Figure 1. In particular, the integration of the engines with increasing bypass ratio represents a challenge for the underwing arrangement of the engine. With increasing aspect ratio and sweep angle of the wing, the design space of the wing planform becomes increasingly

limited because the required center of gravity range determines the positioning of the main landing gear and the position of the aerodynamic center of the wing due to flight stability requirements.

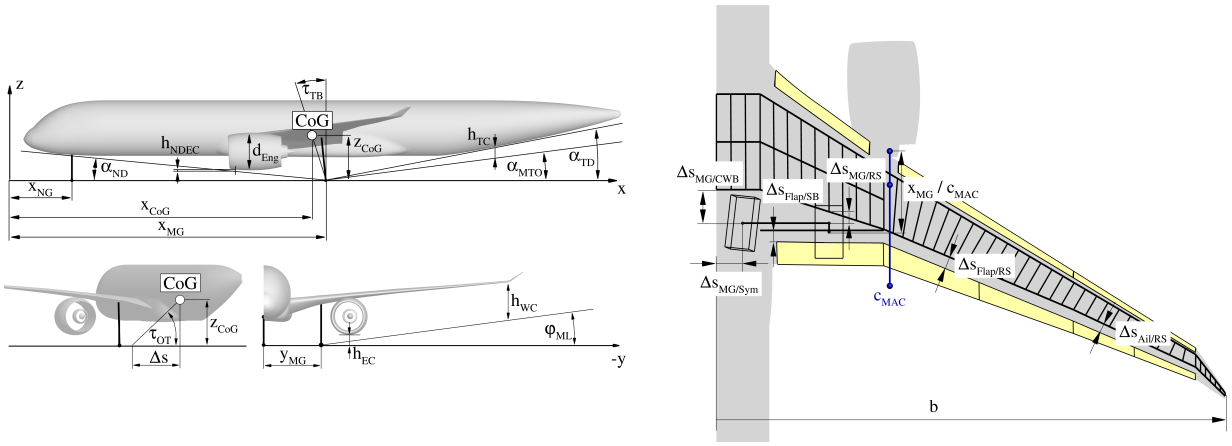

Figure 1 – Geometrical constraints.

The center of gravity range is usually defined as a percentage of the mean aerodynamic chord. With increasing aspect ratio, the mean aerodynamic chord decreases and the sensitivity of the flight characteristics in terms of stability and control increases in relation to the center of gravity position.

2.3 Reynolds Number Effects

The Reynolds numbers Re of the wing sections decreases as the aspect ratio of the wing increases. Equation 3 shows the skin friction coefficient c_f of a flat plate for turbulent flow published by Schlichting [16].

$$c_f = 0.074 Re^{-\frac{1}{5}} \tag{3}$$

Rough estimates based on Equation 3 and the postprocessing of the flow simulations presented in Section 3.4 show a minor impact of wing aspect ratio to friction drag coefficient in the order of less than one drag count.

Another effect of the Reynolds number is its influence on the occurrence of flow separation at adverse pressure gradients $dc_p/dx > 0$. A method for predicting flow separation based on the pressure distribution was published by Stratford [17]:

$$c_p \left(x \frac{dc_p}{dx} \right)^{\frac{1}{2}} \left(10^{-6} Re \right)^{-\frac{1}{10}} = \begin{cases} 0.35 & \text{for } \frac{d^2 c_p}{dx^2} < 0 \quad \text{(concave recovery)} \\ 0.39 & \text{for } \frac{d^2 c_p}{dx^2} \geq 0 \quad \text{(convex recovery)} \quad \text{and} \quad c_p \leq \frac{4}{7} \end{cases} \tag{4}$$

Equation 4 can be used to roughly estimate the order of magnitude of the influence of the Reynolds number on the occurrence of flow separation.

Figure 2 shows the pressure distributions in the outer wing region for the wings of different aspect ratios investigated in Section 3.4. The flow separation depends on the product of the x-coordinate, which starts at the point of pressure rise and the adverse pressure gradient. This product is equal to the absolute value of the local pressure rise and is identical for both airfoils. The estimation based on Equation 4 shows that for the airfoils presented in Figure 2, a reduction of the adverse pressure gradient for the wing with the $30\,\%$ higher aspect ratio in the order of $1 - (Re_{A=13.5}/Re_{A=10.3})^{0.2} \approx 6\,\%$ is required to achieve a comparable robustness against flow separation.

2.4 Static Aeroelastic Effects

With increasing wing aspect ratio and constant wing area, the absolute thickness of the wing decreases, resulting in a lower bending stiffness and a more flexible wing. Due to the bending-torsional coupling of the backward swept wing, the outboard shift of the lift is more pronounced with increasing wing aspect ratio. This results in an outboard shift of the lift as the mass of the aircraft decreases in cruise flight. Each spanwise shift of the lift is associated with a shift in the x-direction due to the

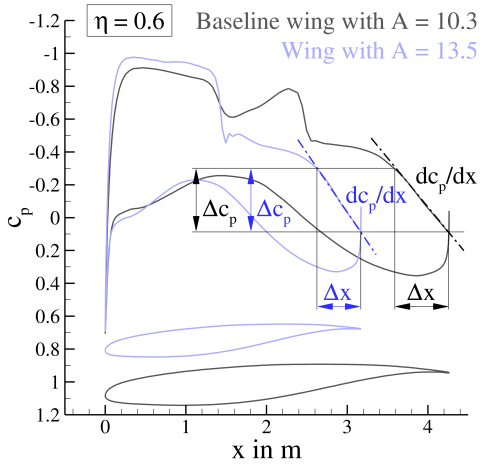

Figure 2 – Pressure coefficient distributions of outer wing section for wings with different aspect ratio.

sweep of the wing, which has an effect on the flight characteristics and trimming of the aircraft. The reduced bending stiffness with increasing wing aspect ratio increases the passive load reduction, which causes a load shift towards the inner wing with increasing loads.
Due to the reduced wing stiffness, the effectiveness of the control surfaces in the outer wing region decreases with increasing wing aspect ratio and the roll control must be taken over by control surfaces further inboard.

2.5 Wing Mass

The wing mass results from structural sizing of the wing box with the maximum loads. The maximum loads are usually determined in a complex loads process. The maneuver loads achieved with the maximum and minimum load factors required by the certification regulations at maximum take-off mass are suitable for estimating the wing mass. As the flexibility of the wing increases, the dependence of the loads on the deformations increases. A good indication of the load on the wing is the spanwise position of the center of lift, which corresponds to the maximum bending moment at the wing root. In addition to the materials used and their material properties, stability criteria and manufacturing boundary conditions also play a central role in the structural sizing of lightweight structures, such as the wings of commercial aircraft. For this reason, the wing mass cannot be determined directly from the maximum loads.
In addition to the maximum loads, the wing mass depends on the wing geometry. The wing box forms the load-bearing structure and its absolute thickness represents the central geometric variable with regard to the wing mass. For a wing section, the dependence of the wing mass m_W can be estimated using the beam theory under pure bending load and a maximum strain allowable $\varepsilon_{Mat,max}$ with the following equation:

$$dm_W \sim t_{covers} \cdot c \cdot \rho_{Mat}\, dy \sim \frac{\rho_{Mat}}{E_{Mat}\, \varepsilon_{Mat,max}} \cdot \frac{M_{x,max}}{t}\, dy \tag{5}$$

The estimated wing mass is proportional to the internal bending moment M_x and inversely proportional to the absolute wing thickness t. The materials used and their properties (density ρ_{Mat} and Young's modulus E_{Mat}) also have a significant influence on the wing mass.
With increasing wing aspect ratio and constant wing area, the wing mass increases due to the reduction in absolute airfoil thickness. Taking realistic geometric constraints into account, Figure 7 shows the distribution of the wing thickness in the spanwise direction resulting from an increase in the wing aspect ratio. The influence of the aeroelastic effects increases with increasing wing aspect ratio due to the lower stiffness. This has a positive effect on the loads during maneuver flight with a swept-back wing because the shift of the center of lift towards the inner wing is more pronounced. As the wing aspect ratio increases, the lift curve slope increases and consequently the load level due to gusts also increases.

2.6 Flutter

In order to investigate flutter sensitivity with respect to aspect ratio, a study has been performed with wings of similar topology and different aspect ratios. In this study, the wing box structure has been sized in a loads process and then examined with regard to flutter speed boundaries. No clear trend could be identified, as the flutter modes depend on the ratio of bending and torsional stiffness, which is not directly influenced by the aspect ratio. The study has been carried out in collaboration with an aircraft manufacturer and the details are not included in this publication.

2.7 Adaptive Wing

With the adaptive wing technology, the spanwise load distribution has to be adapted to the flight condition with the aim of improving cruise flight performance and reducing the structural loads. Multifunctional control surfaces are to be used for the redistribution of the spanwise lift distribution.
In the future, the maximum loads are to be significantly reduced and simultaneously optimum spanwise lift distribution in cruise flight is to be achieved. As a result, the adaptive wing technology is regarded as enabler for wings with higher aspect ratio.
A shift of the center of lift in the spanwise direction is directly related to a shift in the x-direction for a backward swept wing and the resulting consequences for stability and control. This effect is intensified with increasing wing aspect ratio and represents a limitation of the spanwise center of lift shift for higher wing aspect ratios. In particular, the desired shift of the center of lift towards the outer wing in cruise flight to reduce the induced drag leads to an increase in trim drag with increasing aspect ratio. This is due to the fact that the center of lift of the wing moves backwards simultaneously and consequently more downforce is required on the horizontal stabilizer, which must be compensated for by the wing at a given lift.

3. Multidisciplinary Wing Optimizations

An integrated process chain for aero-structural wing optimization based on high fidelity simulation methods has been used for the presented optimizations of the wing planform, the twist distribution and the control surface deflections. A detailed description of the original process chain and their successful application has been published by Wunderlich et al. [13, 18]. The process chain include a mesh deformation techniques for geometry changes and simplified control surface deflections, a landing gear integration, a tail sizing based on handbook methods and a trim drag estimation functionality. The improvements described in the current article relate to the introduction of a component based fluid structure interaction, which allows the accurate consideration of wing deformations in the presence of an engine nacelle.
To investigate the optimum wing aspect ratio for a long-range aircraft, the first step was to optimize the twist distribution of the baseline configuration with a wing aspect ratio of $A_W = 10.3$ in a multidisciplinary process with the objective to achieving the minimum fuel consumption. The wing planform and the airfoil shapes of the baseline configuration result from aero-structural wing optimizations of a wing in conventional fiber composite design (the planform optimization has been published by Wunderlich [19]), which are not the subject of this publication. In this work, an advanced structural concept for the wing box according to Section 3.3.4 has been used, which required the optimization of the baseline configuration.
In the second step, the aero-structural optimization of a wing with an aspect ratio of $A_W = 13.5$ has been performed, whereby in addition to the twist distribution, the control surface deflections have been considered as design parameters to improve the cruise flight performance and to reduce the maneuver loads. The wing planform with this ultra-high aspect ratio is the wing with the highest aspect ratio found by parametric variation of the wing geometry taking geometric constraints into account. The aim of optimizing the twist distribution and the control surface deflections is to determine the optimum lift distribution for each flight condition with regard to minimum fuel consumption. In addition to the flight performance in cruise flight, the structural mass of the wing resulting from the structural sizing, including the wing deformations, is also taken into account.
The final step was an aero-structural optimization of the wing planform, the twist distribution and the control surface deflections. Due to the high number of design parameters and the use of a global

optimization strategy, the optimization has been performed in two stages. In the first stage, the wing planform and the twist distribution have been optimized and in the second stage, the twist distribution and the control surface deflections have been optimized simultaneously.

3.1 Process for Aero-structural Wing Optimization

The process chain applied in the present work is shown in Fig. 3 in the form of XDSM-diagrams (Extended Design Structure Matrix) [20]. In each optimization step, the aircraft description of the baseline configuration is updated according to the current values of the design parameters. The resulting aircraft description is transferred to the subsequent simulation programs using the Common Parametric Aircraft Configuration Schema (CPACS) [21].
In the next step the parametric CAD model is updated, the aerodynamic volume mesh is deformed, and the structural model is generated. The parametric CAD model has been built in the commercial software CATIA® V5, which enables accurate surface representation, and robust and time efficient geometry changes.
In the CFD volume mesh deformation process, the mesh representing the baseline configuration is deformed in parallel for all flight conditions. According to the control surface deflection to be generated, the displacement field of the surface mesh is computed for each flight condition. It is then transferred to the CFD volume mesh using the Elasticity Analogy (EA) mesh deformation method [22] available in the FlowSimulator [23] environment. The used aerodynamic volume mesh consists of $3.5 \cdot 10^6$ points for the half model of the wing body configuration. The wing shape has been discretized with 198 points in each airfoil section and with 162 points in span direction. This mesh resolution represents an appropriate trade-off between accuracy and computing effort for wing optimization.
For the generation of the structural model, the DLR in-house tool DELiS (Design Environment for thin-walled Lightweight Structures) [24] is used. Based on the central data format CPACS, DELiS automatically generates a consistent finite element mesh by using the open-source tool Gmsh [25]. The finite element model is made up of shells elements enriched with physical properties of the wing spars, ribs, and skin cells and finally exported for the commercial FE solver MSC Nastran™. In this work, the structural model consists of 18968 elements for the half model of the wing box.
The fluid-structure coupling loop is marked with a rounded yellow box and the values of the design mission lift-to-drag ratio, the wing mass and the objective function value are evaluated for the convergence examination.
For all flight conditions the aerodynamic forces and coefficients are computed using RANS-based CFD simulations. The flow simulations are performed by using the DLR TAU-Code [26, 27] which is integrated in the HPC framework FlowSimulator [28]. The solver's capabilities with respect to accurate flow predictions, also in near off-design regions, have been demonstrated in numerous publications, including those of the AIAA Drag Prediction Workshop Series [29]. The approach ensures that flight performance under cruise flight conditions and selected maneuver loads with consideration of flow separations are analyzed accurately and efficiently.
Based on the aerodynamic loads computed for the flight conditions considered, the wing-box structure is sized. Within the structural analysis and sizing process the disciplinary objective is to fulfill the structural constraints in terms of failure criteria and converge the margins of safety (MoS) and wing mass. Hence, the structural analysis and sizing process represents a subspace optimization. Different design criteria are applied to ensure a valid structural design. As proposed by Dähne et al. [30] for stiffened panels, the criteria for strength, maximum strain, and local and global buckling are used for skin and all stringer components. The main results of this process are the wing mass and the deformed wing shapes for the flight conditions considered. The structural analysis and sizing process uses the commercial software MSC Nastran™ for computing the internal loads and stresses. The commercial software HyperSizer® is applied for sizing the composite wing box.
The structural deformations form the input for the CFD volume mesh deformation. A mesh deformation method based on radial basis functions (RBF) [31] available in the FlowSimulator is used.
Afterwards, the objective function is evaluated and the convergence criteria of the static aeroelastic analysis are examined. The convergence criteria are based on monitoring the changes in lift-to-drag

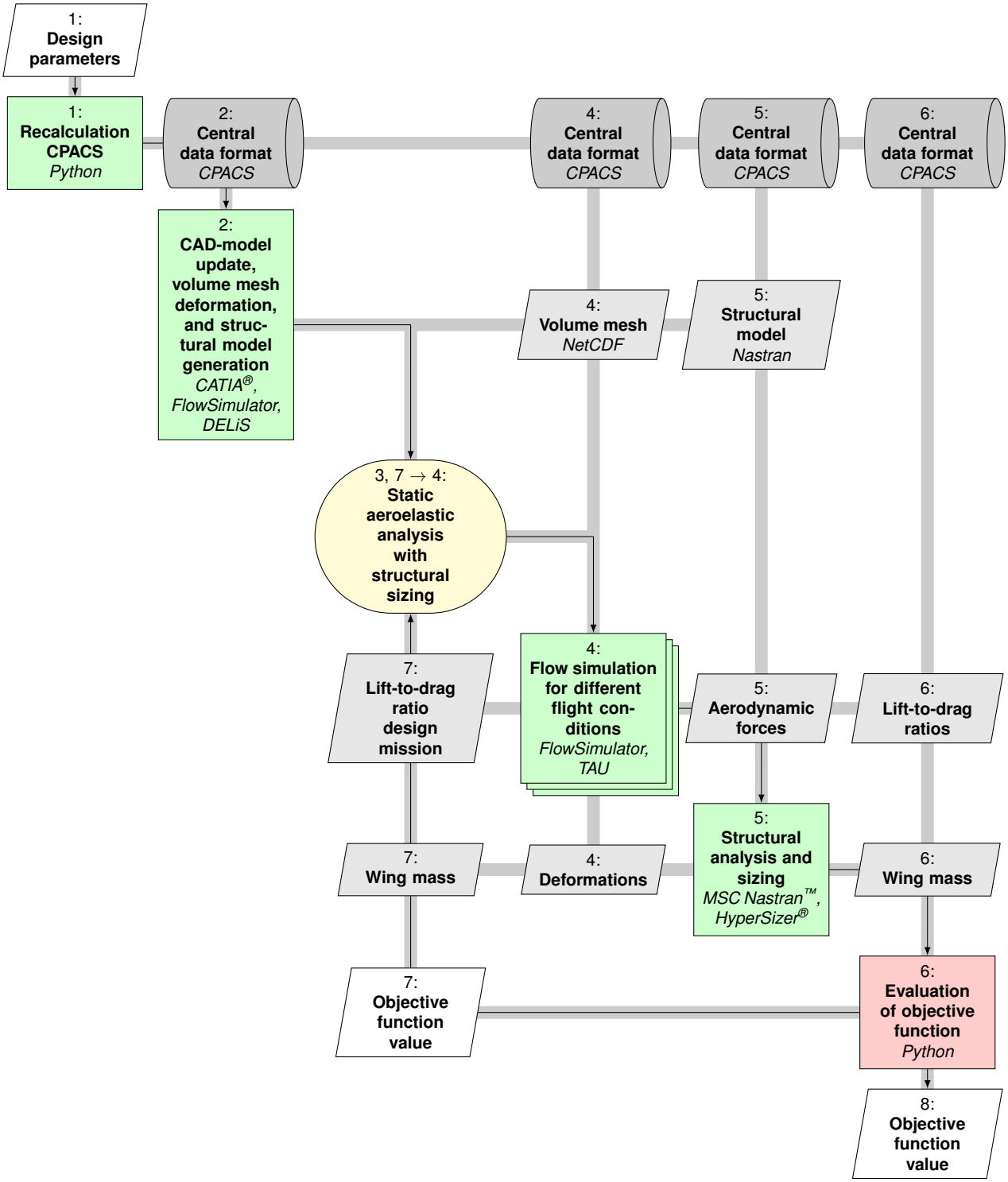

Figure 3 – Flow chart of the process chain for aero-structural wing analysis.

ratio, wing mass, and objective function value. Once convergence of the fluid-structure coupling loop is reached, the objective function value is given to the global optimizer.

3.2 Global optimization strategy

For the wing optimizations in this work an in-house surrogate-based optimization (SBO) method implemented by Wilke [32] has been selected. This global optimization strategy represents an adequate compromise between exploring the design space and locating the optimum.

The selected optimization method is an implementation of the optimization method EGO (Efficient Global Optimizer), which has been introduced by Jones et al. [33] and is discussed in Forrester et

al. [34]. At the beginning of the optimization a design of experiments (DoE) for a selected number of samples is performed. In this work, the central Voronoi tessellated (CVT) Latin hypercube [35] has been selected as primary DoE technique. For the calculated objective function value and for each selected constraint, a surrogate model based on kriging [36] is built. These surrogate models are able to model the non-linear behaviour of the objective and constraints. Additionally, a statistical error estimation is included.
Based on the surrogate models of the objective function and constraints, a hybrid optimization strategy is used to find the optimum in terms of expected improvement (EI), which combines the predictions of objective function value and model error. The hybrid optimization strategy starts with a global optimization method and the localization of the optimum is improved by the application of a local optimization method. For the global optimization the differential evolutionary (DE) algorithm published by Storn and Price [37] is used. The simplex pattern search method from Nelder and Mead [38] has been selected for the local search in the surrogate models. For the resulting global optimum in terms of expected improvement a recalculation with the physical model is performed. The result of this recalculation is then used to improve the surrogate models for the objective function value and constraints. The described optimization procedure is iterated until convergence is reached.

3.3 Design Task

The design task describes the objective function, the design space, and the constraints. In this work the wing design for a long-range passenger aircraft has been selected.

3.3.1 Objective Function, Flight Missions and Load Cases

The objective function of the multi-mission aero-structural wing optimizations is the combined fuel consumption per range and payload of three selected flight missions. Thus, the combined fuel consumption is the weighted sum of the fuel consumption of the corresponding missions as given in Equation (6).

$$\frac{m_F}{R\,m_P} = \sum_i w_i \left(\frac{m_F}{R\,m_P} \right)_i \tag{6}$$

Table 2 provides an overview of the selected flight missions and weighting factors. With the selected weighting factors, the expected relative frequency of the missions in airline operation has been taken into account.

Flight missions		**Study mission (FC1)**	**High speed mission (FC2)**	**Design mission (FC3)**
Weighting factor	w_i	0.6	0.1	0.3
Cruise Mach number	Ma	0.83	0.85	0.83
Range	R	4000 nm (7408 km)	4000 nm (7408 km)	6000 nm (11 112 km)
Payload	m_P	40 800 kg	40 800 kg	-
Reserve fuel ratio	$m_{F,res}/m_F$	0.1400	0.1400	0.1000
Flight load case		**Pull up maneuver (LC1)**	**Push over maneuver (LC2)**	**Roll maneuver (LC3)**
Altitude	H	0 m	3048 m	0 m
Mach number	Ma	0.552	0.655	0.552
Lift coefficient	C_L	0.744	−0.305	0.593
Load factor	n	2.5	−1.0	2.0

Table 2 – Flight missions and flight load cases.

For the study and design mission the design Mach number of the Airbus A330 has been selected. The design mission range is set to $6000\,\mathrm{nm}$ and the corresponding payload is a result of the static aeroelastic analysis. The selection of range and payload for the study mission is based on a typical long-range mission with a passenger load factor of 0.85 and represents the mission for which the aircraft will be optimized primarily. The difference between high speed and the study mission is the increased cruise Mach number to consider off-design conditions in the wing optimization.
For the structural sizing of the wing box the maneuver load cases with the maximum loads have to be defined. These maneuver load cases have been derived from the flight envelope limits and the limits

of the maneuvering load factor resulting from the certification regulations CS-25/FAR 25. In Table 2 an overview of the selected maneuver load cases is given. In addition to the presented maneuver flight load cases a touch down load case has been introduced to consider the landing gear loads in the wing box sizing.
A conceptual design model has been used to calculate the fuel consumption of the individual flight missions. In this model, the cruise segment of the mission is described by the well-known Breguet range equation. The thrust-specific fuel consumption has been derived from the engine map of a geared turbofan provided by the DLR-Institute of Propulsion Technology. The lift-to-drag ratio in cruise is obtained from the aerodynamic coefficients of the flow simulation for the wing-fuselage-engine configuration, the estimated aerodynamic coefficients of the tailplane and the specified residual drag and residual thrust coefficients. The longitudinal trim of the aircraft for the given center of gravity position is taken into account. Further details on the models and equations used are described by Wunderlich et al. [13, 18].

3.3.2 Design Parameters and Constraints

An overview of the used design parameters is given in Figure 4. The baseline aircraft configuration results from an aero-structural optimization of the twist distribution for a given wing planform and the advanced structural concept of the wing box described in Section 3.3.4. The twist angles ε_i specified in Table 3 have been used as design parameters to optimize the twist distribution. For the optimization of the wing with ultra-high aspect ratio, the deflection angles δ_j of five control surfaces actuated in different flight conditions have been used as design parameters in addition to the twist distribution.

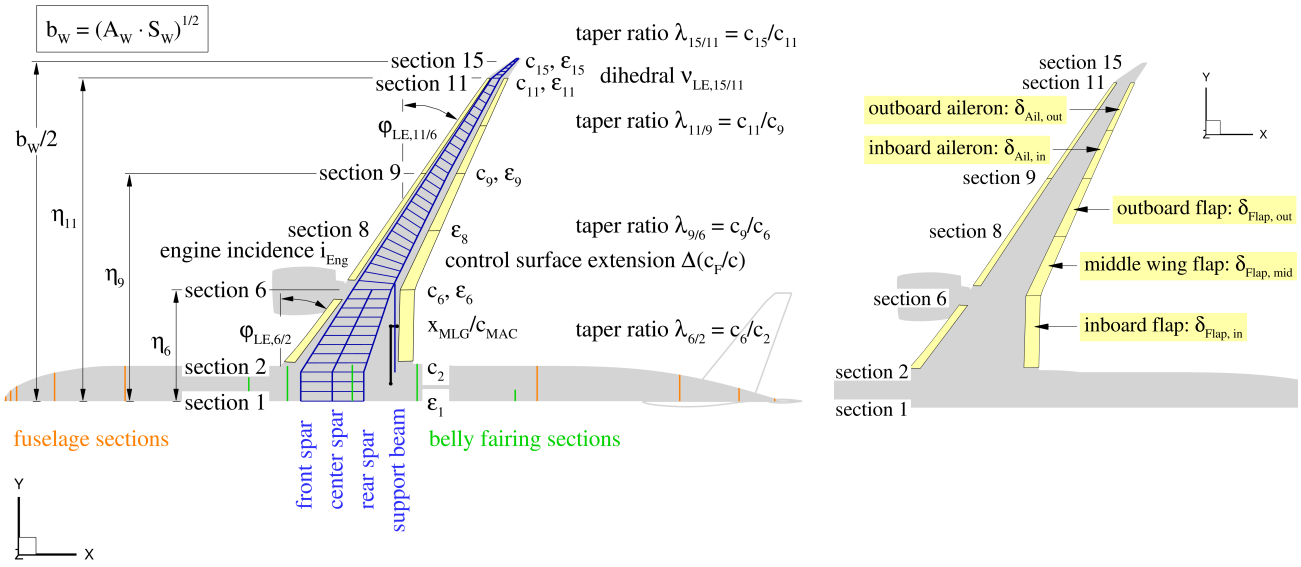

Figure 4 – Design parameters.

As already described, the optimization of the wing planform and the control surface deflections has been performed in two stages. In the first stage, the parameters of the wing planform and the twist distribution have been optimized. In the second stage, an optimization has been performed with the identical design parameters as in the optimization of the wing with the ultra-high aspect ratio according to Table 3. The definition and designation of the design parameters are given in Figure 4.
The wing airfoils and fuselage shape have been kept constant during the wing optimizations. In addition the maximum take-off mass, the maximum payload, and specific masses of the leading and trailing edges are constant. The wing mass is a result of the structural sizing of the wing box and the tail mass is estimated by scaling the tail mass of the reference aircraft with the tail surface ratio after tail sizing. During optimization, the required fuel tank volume is calculated for all selected flight missions and compared to the usable fuel tank volume.
For the integration of the landing gear, the control surfaces and the engine, the geometrical constraints shown in Figure 1 are taken into account with the given value ranges specified in Table 4.

	Twist optimization (Baseline)	**Control surface deflection optimization A = 13.5**	**Planform and control surface deflection optimization**
Wing area	-	-	S_W
Aspect ratio	-	-	A_W
Outboard kink position	-	-	η_9
Winglet position	-	-	η_{15}
Winglet dihedral angle	-	-	$\nu_{15/11}$
Taper ratios	-	-	$\lambda_{6/2}$, $\lambda_{9/6}$, $\lambda_{11/9}$, $\lambda_{15/11}$
Leading edge sweep angles	-	-	$\varphi_{LE,6/2}$, $\varphi_{LE,11/6}$
Twist distribution	ε_1, ε_6, ε_8, ε_9, ε_{11}	ε_1, ε_6, ε_8, ε_9, ε_{11}, ε_{15}	ε_1, ε_6, ε_8, ε_9, ε_{11}, ε_{15}
Control surface extension	-	-	$\Delta(c_F/c)$
Main gear position	-	-	x_{MLG}/c_{MAC}
Engine angle of incidence	-	i_{Eng}	i_{Eng}
Control surface deflections for cruise flight cases and maneuver load cases (see Table 2)	- - - - -	FC1: $\delta_{Flap,in}$ FC2: $\delta_{Flap,in}$, $\delta_{Flap,mid}$, $\delta_{Flap,out}$ FC3: $\delta_{Flap,in}$ LC1: $\delta_{Flap,in}$, $\delta_{Ail,in}$, $\delta_{Ail,out}$ LC2: $\delta_{Flap,in}$, $\delta_{Ail,in}$, $\delta_{Ail,out}$	FC1: $\delta_{Flap,in}$ FC2: $\delta_{Flap,in}$, $\delta_{Flap,mid}$, $\delta_{Flap,out}$ FC3: $\delta_{Flap,in}$ LC1: $\delta_{Flap,in}$, $\delta_{Ail,in}$, $\delta_{Ail,out}$ LC2: $\delta_{Flap,in}$, $\delta_{Ail,in}$, $\delta_{Ail,out}$
Number of design parameters	5	18	$19+18$

Table 3 – Design parameters.

Masses	Maximum take-off mass	$220000\,\mathrm{kg}$
	Maximum payload	$54000\,\mathrm{kg}$
	Residual mass ratio (fuselage, operating items)	0.3952
	Specific mass of leading edge	$30\,\mathrm{kg/m^2}$
	Specific mass of trailing edge	$50\,\mathrm{kg/m^2}$
	Center of gravity position	$36\,\%\ c_{MAC}$
Geometry	Fuel tank volume	$V_F \geq V_{F,req}$
	Outer main gear wheel span (ICAO Code E)	$9\,\mathrm{m} \leq 2\,y_{MG} \leq 14\,\mathrm{m}$
	Nose gear static load ratio	$5\,\% \leq F_{NG}/mg \leq 20\,\%$
	Tip back angle	$\tau_{TB} \geq 15°$
	Overturn angle	$\tau_{OT} \leq 63°$
	Take-off rotation angle (with $0.25\,\mathrm{m}$ tail clearance)	$\alpha_{TO} \geq 10°$
	Castor angle of main gear leg	$83° \leq \tau_{Cas} \leq 90°$
	Distance between main gear and rear spar	$0.6\,\mathrm{m} \leq \Delta s_{MG/RS} \leq 1.6\,\mathrm{m}$
	Distance between flap and support beam	$\Delta s_{Flap/SB} \geq 0.2\,\mathrm{m}$
	Distance between flap and rear spar	$\Delta s_{Flap/RS} \geq 0.065\ c_{MAC}$
	Distance between aileron and rear spar	$\Delta s_{Ail/RS} \geq 0.04\ c_{MAC}$
Aerodynamics	Residual drag coefficient	0.0018
	Residual thrust coefficient (through-flow nacelle)	0.0030

Table 4 – Constraints.

The aerodynamic coefficients in the aerodynamic simulation are corrected with a constant residual drag coefficient to account for drag from components that are neglected in the simulation, such as the engine pylon and flap track fairings. An additional residual thrust has been introduced to correct the coefficients in the simulation with a flow-through nacelle. Fig. 4 summarizes the constraints that have been taken into account.

3.3.3 Adaptive wing

Adaptive wing technology describes the controlled adaptation of the wing shape to different flight conditions with the aim of improving cruising performance and reducing loads in order to reduce mass

and increase passenger comfort. In this work multi-functional control surfaces at the wing trailing edge have been integrated into the aircraft configuration to introduce variable camber technology.
The potential of fuel burn reduction due to cruise flight performance improvement has been shown in the publication of Wunderlich and Siebert [12] for a long-haul passenger aircraft with identical top level aircraft requirements (TLARs). In comparison to this previous work, the technology of active maneuver load alleviation by the usage of trailing edge control surfaces and the structural sizing of the wing box have been added. The selection of control surfaces for cruise flight performance improvements has been derived from the results of this previous work to overcome the practical limitations in the number of design parameters.

3.3.4 Structural concept

In this work an advanced structural concept of increased strain allowable and post-buckling has been selected. The classic skin-dominated design of the covers has been replaced by a stringer-dominated design. The selected values of the strain allowable and the corresponding percentage ply share of the covers, spars and ribs based on the calculations of damaged tolerance design allowables published by Bogenfeld et al. [7]. Furthermore, the structural technology of post-buckling has been introduced, which permits local buckling after limit load.
Figure 5 summarizes the structural concept used with increased strain allowable and post-buckling.

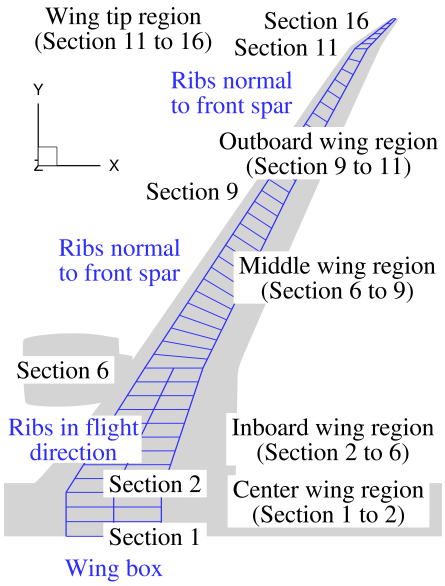

Structural concept of the covers		Stringer-dominated design
Stringer type		T-stringer
Ribs spacing	Center wing	0.85 m
	Inboard wing	0.85 m
	Middle wing	0.75 m
	Outboard wing	0.75 m
	Wing tip	0.50 m
Percentage ply share $0°/\pm45°/90°$	Covers	20/70/10
	Spars	20/70/10
	Ribs	20/70/10
	Stringers	70/20/10
Strain allowable	Tension	6100 µm/m
	Compression	4400 µm/m
	Shear	8800 µm/m
Local buckling		Local buckling after limit load ("post-buckling")

Figure 5 – Structural concept of increased strain allowable and post-buckling.

3.4 Results

The starting point for multidisciplinary wing optimization is the baseline configuration, which is the result of a twist distribution optimization after introducing the advanced structural concept of the wing box as described in Section 3.3.4. The wing of the baseline configuration has been optimized using state-of-the-art technology for active maneuver load reduction (MLA). The ailerons have been used with the deflection angles given in Table 6.
Starting from the baseline configuration, the wing planform geometry with ultra-high aspect ratio has been introduced, taking into acount the adaptive wing technology, and an aero-structural wing optimization of the twist distribution and the control surface deflections has been performed.
In the next wing optimization, the optimal wing planform geometry including the wing aspect ratio has been determined taking into account the adaptive wing technology. Due to the high number of design parameters for the use of a surrogate-based global optimization strategy, the optimization has been performed in two stages as mentioned before.

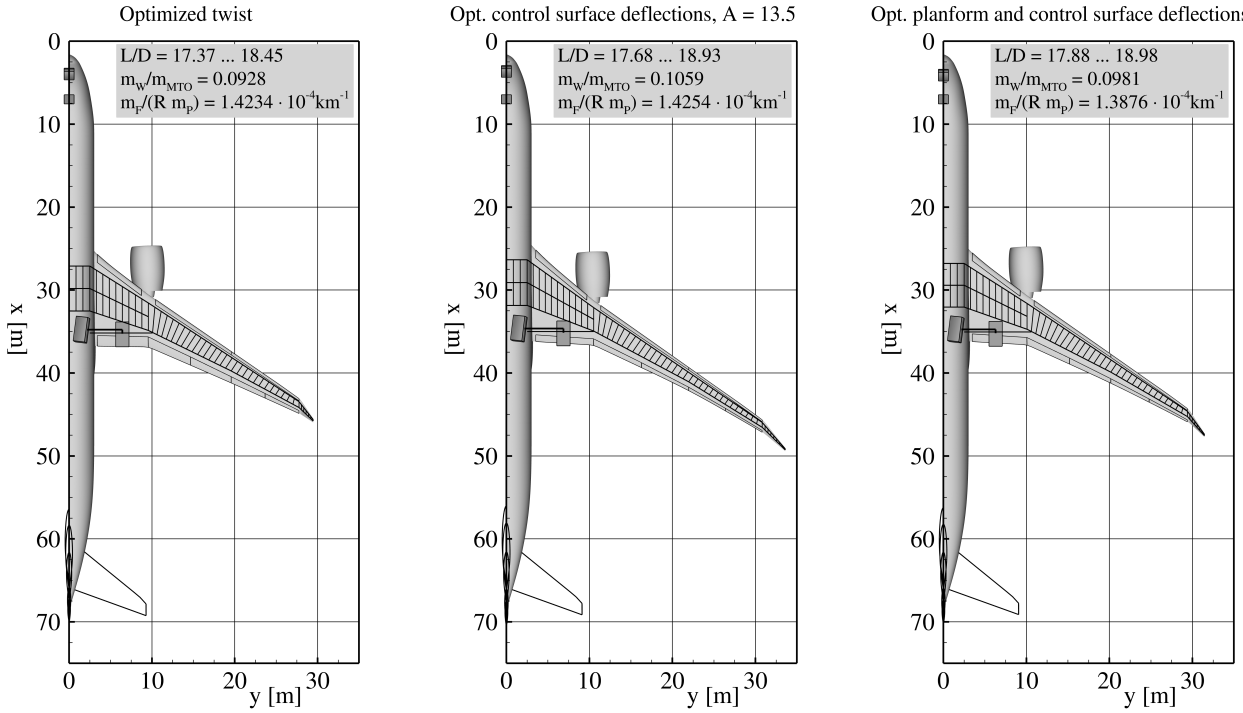

Figure 6 – Wing planforms of baseline and optimized wings.

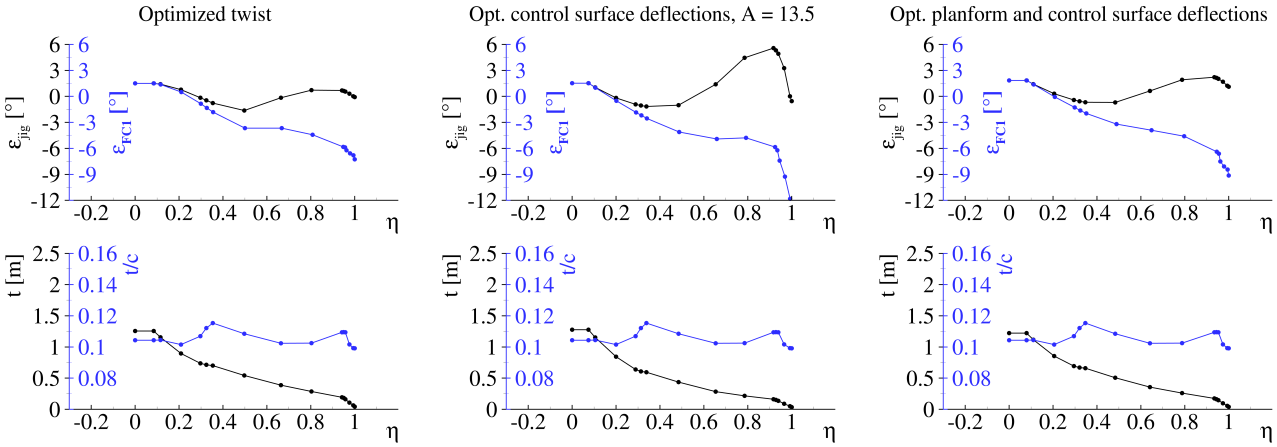

Figure 7 – Twist and thickness distributions of optimized wings.

The corresponding results in Table 6 show an increase in the lift-to-drag ratio between 1.8 % and 2.9 % depending on the flight mission considered for the ultra-high aspect ratio wing compared to the baseline configuration. This increase is in the order of the estimated value 3.3 % in Section 2.1 for the assumption of constant center of lift under cruise flight conditions. The wing mass has been increased by 14.1 % compared to the baseline configuration (see Table 5), although the adaptive wing technology has been added to the ultra-high aspect ratio wing. The resulting fuel consumption in Table 6 for the ultra-high aspect ratio configuration shows advantages for the study mission and disadvantages for the design mission compared to the baseline configuration. This leads to a similar objective function value in the combined fuel consumption.

By optimizing the wing planform, it was possible to maintain the high lift-to-drag ratio of the wing with ultra-high aspect ratio as shown in Table 6 and simultaneously limit the increase in the wing mass to 5.7 % (see Table 5). The high lift-to-drag ratio can be explained by the more favorable lift distribution in cruise flight as shown in Figure 10, which has even higher Oswald's effeciency factors compared to the baseline configuration due to the use of adaptive wing technology. Table 6 shows the Oswald's efficiency factors for all flight missions investigated.

The optimized twist distributions of the configurations with adaptive wing technology in Figure 7 show

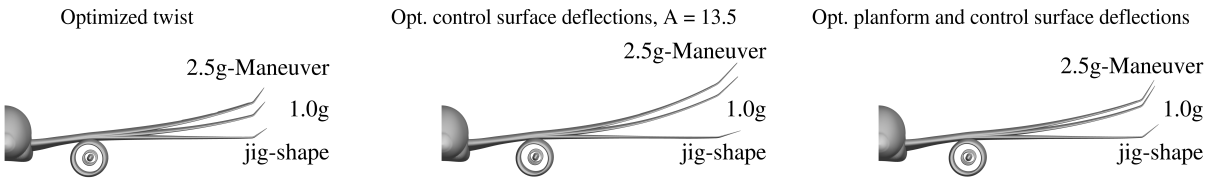

Figure 8 – Wing deformations for cruise and maneuver flight of baseline and optimized wings.

greater differences between the twist angles in the unloaded state ("jig shape") in black compared to cruise flight in blue due to the increase in wing deformations shown in Figure 8. The differences in the wing deformations between the $1.0\,g$ cruise flight and the $2.5\,g$ maneuver flight are an indicator of how well the lift adaptation works through the use of optimized control surface deflections.

		Baseline	Optimized control surface deflections, A = 13.5	Opt. planform and control surface deflections
Wing geometry				
Wing area	S_W	337.3 m^2	333.9 m^2	334.6 m^2
Wingspan	b_W	58.89 m	67.14 m	62.85 m
Mean aerodynamic chord	$c_{MAC,W}$	7.58 m	7.37 m	7.27 m
Aspect ratio	A_W	10.283	13.503	11.806
Taper ratio	λ_W	0.036	0.029	0.033
Leading edge sweep angle	$\varphi_{W,LE}$	34.5°	35.2°	35.1°
Flap spar offset	$\Delta s_{Flap/RS}$	0.61 m	0.56 m	0.69 m
Aileron spar offset	$\Delta s_{Ail/RS}$	0.31 m	0.31 m	0.34 m
Useable fuel tank volume	V_F	98.49 m^3	94.22 m^3	93.51 m^3
Tail geometry				
Horizontal tail area	S_{HTP}	68.9 m^2	66.3 m^2	65.6 m^2
Vertical tail area	S_{VTP}	49.4 m^2	55.7 m^2	52.3 m^2
Landing gear				
Landing gear wheel base	l_{LG}	28.33 m	28.21 m	28.27 m
Outer main gear wheel span	$2\,y_{MG}$	12.85 m	13.74 m	12.57 m
Nose gear static load factor	$F_{NG}/(m\,g)$	0.056, …, 0.078	0.053, …, 0.074	0.056, …, 0.076
Tipback angle	τ_{TB}	17.2°, …, 23.6°	15.4°, …, 21.3°	17.5°, …, 23.8°
Overturn angle	τ_{OT}	41.0°, …, 41.0°	40.8°, …, 40.9°	40.7°, …, 40.8°
Maximum takeoff rotation angle	α_{MTO}	10.9°	11.6°	10.6°
Main gear spar offset	$\Delta s_{MG/RS}$	0.95 m	1.10 m	1.35 m
Main gear flap offset	$\Delta s_{Flap/SB}$	0.30 m	0.38 m	0.22 m
Masses				
Mass of covers	$m_{W,covers}$	5969 kg	7718 kg	6664 kg
Mass of spars	$m_{W,spars}$	1987 kg	2352 kg	2065 kg
Mass of ribs	$m_{W,ribs}$	1565 kg	1824 kg	1729 kg
Wing box mass[a]	$m_{W,box}$	11 900 kg	14 867 kg	13 074 kg
Wing mass ratio	m_W/m_{MTO}	0.0928	0.1059	0.0981
Operational empty mass ratio	m_{OE}/m_{MTO}	0.5047	0.5183	0.5099

[a] Values are scaled by a factor of 1.25 to account for additional masses of local reinforcements and fasteners.

Table 5 – Results overview of wing optimizations (geometry and masses).

Figure 10 presents the lift force and lift coefficient distributions for the baseline configuration and the optimized configurations with adaptive wing technology. The corresponding center of lift is shown as a black circle and the value is given in Table 6. For each lift distribution, the related elliptical lift distribution is shown by a dashed line, and the corresponding center of lift is indicated by a gray square. The elliptical lift distribution is the optimum for planar wings in terms of lift induced drag. The increase in the lift-to-drag ratio in cruise flight can be explained by the combination of increased wing aspect ratio and Oswald's efficiency factor with regard to the induced drag (see Equation 1). The outboard shift of lift is aerodynamically limited by an increase in the local lift coefficient (blue line in

		Baseline	Optimized control surface deflections, A = 13.5	Opt. planform and control surface deflections
Maneuver n=2.5				
Control surface deflections	$\delta_{Flap,in}$	$0.0°$	$+18.5°$	$+15.2°$
	$\delta_{Aileron,in}$	$-10.0°$	$-12.1°$	$-12.0°$
	$\delta_{Aileron,out}$	$-15.0°$	$-14.5°$	$-20.0°$
Angle of attack	α	$8.0°$	$7.0°$	$6.4°$
Center of lift	η_{CoL}	0.3386	0.2916	0.3071
Maneuver n=-1.0				
Control surface deflections	$\delta_{Flap,in}$	$0.0°$	$-11.4°$	$-19.5°$
	$\delta_{Aileron,in}$	$+5.0°$	$+17.9°$	$+19.9°$
	$\delta_{Aileron,out}$	$+10.0°$	$+10.3°$	$+13.9°$
Angle of attack	α	$8.0°$	$7.0°$	$6.4°$
Center of lift	η_{CoL}	0.3386	0.2916	0.3071
Study mission				
Control surface deflections	$\delta_{Flap,in}$	$0.0°$	$-0.9°$	$-2.6°$
Angle of attack	α	$3.6°$	$4.4°$	$4.1°$
Lift-to-drag ratio	L/D	18.32	18.86	18.87
Center of lift	η_{CoL}	0.3804	0.3572	0.3802
Oswald's efficiency factor	e	0.8453	0.7550	0.8619
Fuel consumption	$m_F/(Rm_P)$	$1.3819\times10^{-4}\,\mathrm{km}^{-1}$	$1.3678\times10^{-4}\,\mathrm{km}^{-1}$	$1.3509\times10^{-4}\,\mathrm{km}^{-1}$
High speed mission				
Control surface deflections	$\delta_{Flap,in}$	$0.0°$	$-1.7°$	$-0.9°$
	$\delta_{Flap,mid}$	$0.0°$	$+0.5°$	$+0.2°$
	$\delta_{Flap,out}$	$0.0°$	$-2.4°$	$+0.5°$
Angle of attack	α	$3.4°$	$4.3°$	$3.6°$
Lift-to-drag ratio	L/D	17.37	17.68	17.88
Center of lift	η_{CoL}	0.3790	0.3545	0.3740
Oswald's efficiency factor	e	0.8404	0.7386	0.8443
Fuel consumption	$m_F/(Rm_P)$	$1.4473\times10^{-4}\,\mathrm{km}^{-1}$	$1.4484\times10^{-4}\,\mathrm{km}^{-1}$	$1.4147\times10^{-4}\,\mathrm{km}^{-1}$
Design mission				
Control surface deflections	$\delta_{Flap,in}$	$0.0°$	$-1.3°$	$-1.7°$
Payload	m_P	38 479 kg	36 875 kg	38 854 kg
Used fuel tank volume ratio	$V_{F,req}/V_F$	0.8946	0.9167	0.9218
Angle of attack	α	$3.8°$	$4.5°$	$4.1°$
Lift-to-drag ratio	L/D	18.45	18.93	18.98
Center of lift	η_{CoL}	0.3781	0.3552	0.3744
Oswald's efficiency factor	e	0.8408	0.7481	0.8484
Fuel consumption	$m_F/(Rm_P)$	$1.4986\times10^{-4}\,\mathrm{km}^{-1}$	$1.5329\times10^{-4}\,\mathrm{km}^{-1}$	$1.4520\times10^{-4}\,\mathrm{km}^{-1}$
Objective				
Combined fuel consumption	$m_F/(Rm_P)$	$1.4234\times10^{-4}\,\mathrm{km}^{-1}$	$1.4254\times10^{-4}\,\mathrm{km}^{-1}$	$1.3876\times10^{-4}\,\mathrm{km}^{-1}$
CO_2 emissions per passenger kilometres[a]	$m_{CO2}/(R\,m_P)$	$47.1\,\mathrm{g_{CO2}/pkm}$	$47.1\,\mathrm{g_{CO2}/pkm}$	$45.9\,\mathrm{g_{CO2}/pkm}$

[a] Values of $3.15\,\mathrm{kg_{CO2}/kg_{Fuel}}$ for a turbofan engine [39] and $105\,\mathrm{kg}$ for the passenger mass with baggage are assumed.

Table 6 – Results overview of wing optimizations (flight missions, load cases and objective).

Figure 10) at the outer wing and the corresponding non-linear increase in transonic wave drag. Figure 9 presents the isentropic Mach number distributions of the baseline configuration and the optimized configurations with adaptive wing technology for the study mission. The double shock system of the baseline wing has been significantly improved by using the control surface deflections to optimize the lift distributions. The improvements in cruise performance in terms of lift-to-drag ratio result from the optimum compromise between induced and transonic wave drag.

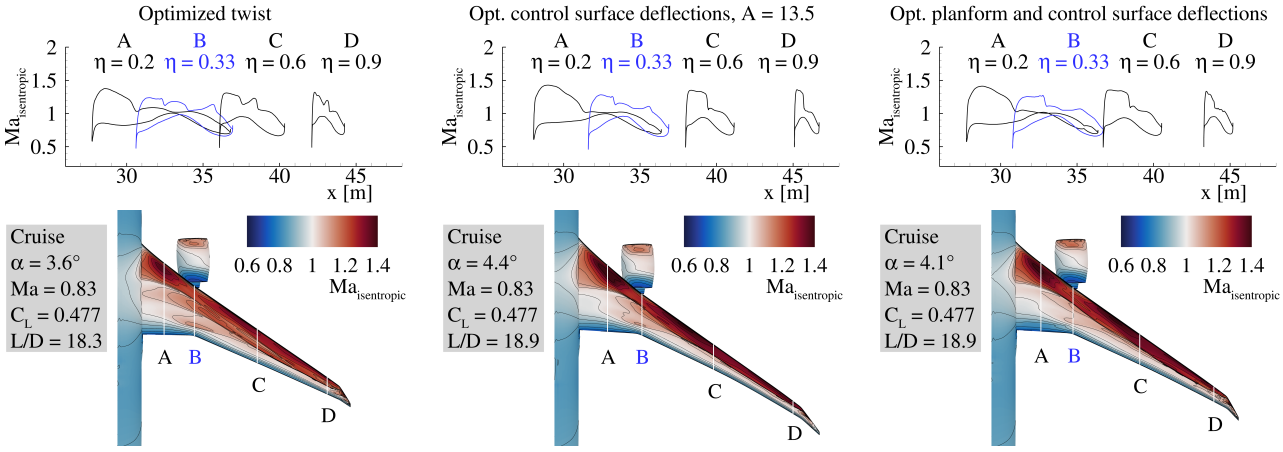

Figure 9 – Isentropic Mach number distributions for cruise flight of baseline and optimized wings.

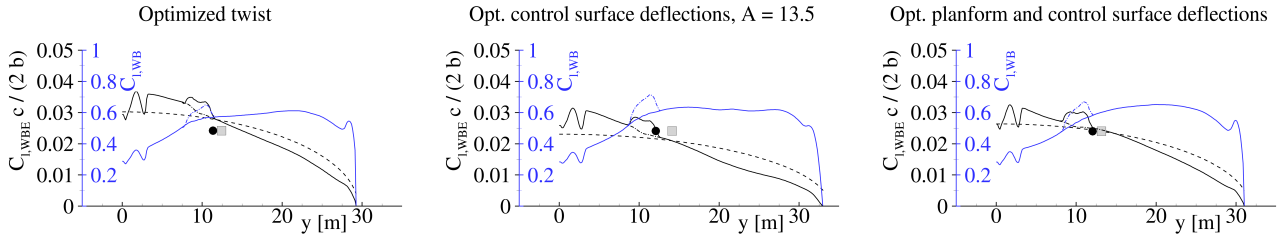

Figure 10 – Lift and lift coefficient distributions for cruise flight of baseline and optimized wings.

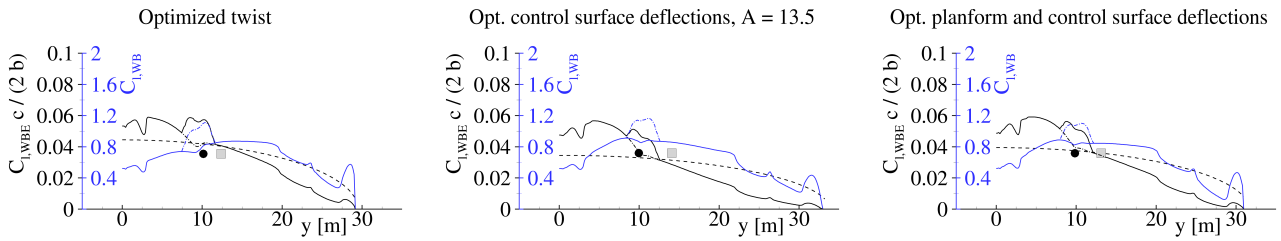

Figure 11 – Lift and lift coefficient distributions for maneuver flight of baseline and optimized wings.

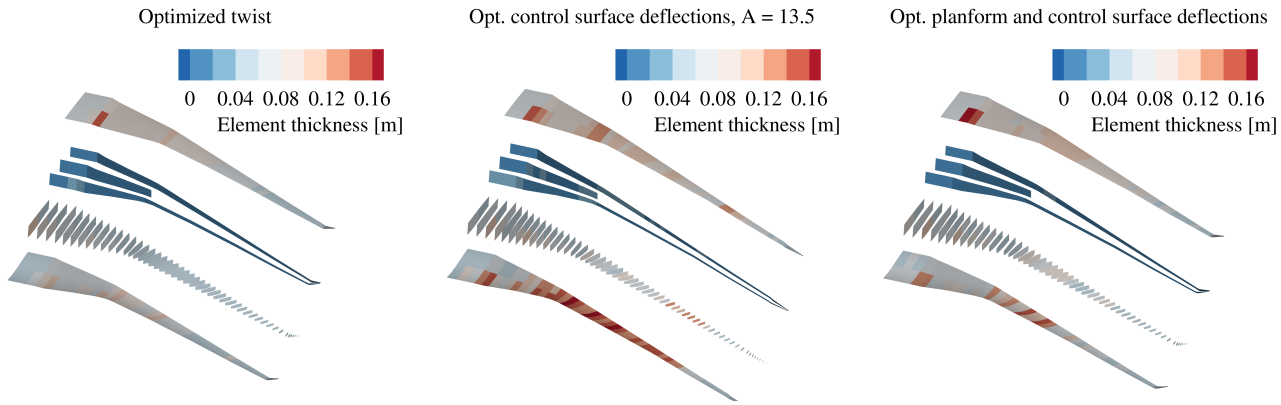

Figure 12 – Wing box element thickness (skin thickness + stringer height) distributions of baseline and optimized wings.

Figure 11 shows the lift distributions for the maneuver flight with a load factor of $n = 2.5$, which is decisive for the structural sizing. Here, the pronounced shift of the lift towards the inner wing becomes clear. This shift significantly reduces the aerodynamic loads and is due to the aeroelastic effects of the backward swept wing and the control surface deflections for load reduction. The resulting element thickness distributions are shown in Figure 12 for the baseline configuration and the optimized configurations with adaptive wing technology. In Table 5 the corresponding mass breakdown of the wing box is given. An increase in wing aspect ratio leads to an increase in wing mass, which can be significantly reduced by introducing the active maneuver load reduction of the adaptive wing.

3.5 Technology assessment of higher wing aspect ratios

The results presented show the potential of higher wing aspect ratios for long-range commercial aircraft in terms of reducing fuel consumption and CO_2 emissions. The optimum wing aspect ratio results from an aero-structural wing optimization taking into account the technology of the adaptive wing and an advanced structural concept. With a value in the order of $A_W \sim 12$, the optimum wing aspect ratio is above the values of modern long-range commercial aircraft, which have aspect ratios in the range of $8 < A_W < 10$. Figure 13 shows the fuel consumption, the lift-to-drag ratio and the wing mass ratio as a function of the wing aspect ratio for all analyzed wing geometries. The resulting fuel consumption has a relatively low sensitivity to the wing aspect ratio. This is due to the counteracting influence of wing aspect ratio on aerodynamic performance and structural mass.

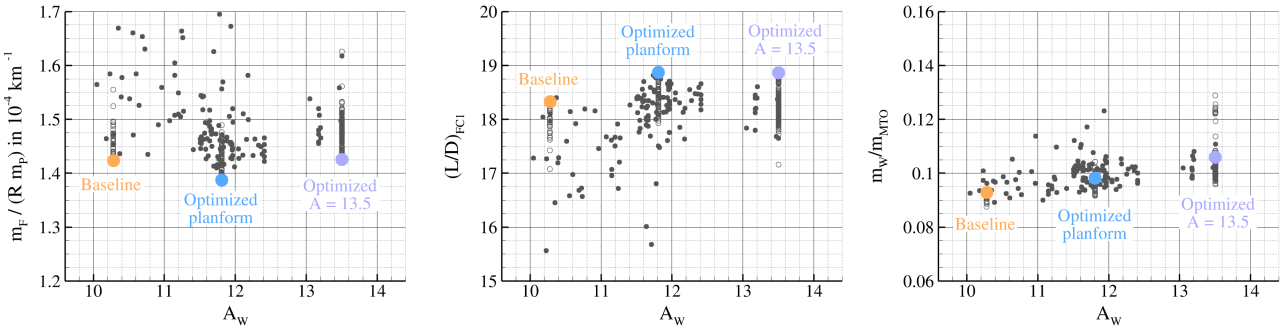

Figure 13 – Optimization results for the combined fuel consumption, lift-to-drag ratio and wing mass ratio as a function of aspect ratio.

Not all aspects could be taken into account in the results shown and uncertainties remain in the statements made with regard to the low number of considered load cases, the limitations of the design space and the specification of the constraints.

4. Conclusion and Outlook

In this work, the potential of higher wing aspect ratios to improve the efficiency of long-range aircraft has been investigated. An integrated process for aero-structural wing optimization based on high fidelity simulation methods has been used to accurately model the flight physics of transonic cruise flight and the structural sizing of the composite wing box. The comparison of optimization results with the same objective function and constraints allows a proper technology assessment.

The introduction of an advanced structural concept and the technology of adaptive wing to improve cruise flight performance and reduce maneuver loads are enablers for higher wing aspect ratios. The optimized wing shows an increased wing aspect ratio of $A_W = 11.8$, which is $14.8\,\%$ higher than the aspect ratio of the baseline configuration. A further increase of the wing aspect ratio to a value of $A = 13.5$ shows no further improvements in the aero-structural optimization.

The increased wing mass of this ultra-high aspect ratio wing leads to optimized lift-distributions with a significantly reduced Oswald's efficiency factor and no further improvements of the lift-to-drag ratio. With the geometrical constraints taken into account, this further increase in wing aspect ratio leads to an increase in combined fuel consumption. The fuel consumption depends on the mission range and therefore an increase in the optimum wing aspect ratio is to be expected if the range requirements are reduced.

In the future, the design space has to be expanded by additionally considering the airfoil shape in the aero-structural wing optimization. Furthermore, the alternative of integrating the main landing gear into the fuselage has to be investigated in order to quantify the potential of the additional geometric freedom in the wing geometry.

5. Acknowledgments

The author would like to thank Andreas Schuster and Sascha Dähne from the DLR-Institute of Lightweight Systems for providing the structure model generation tool and the structural analysis and sizing process to perform the aero-structural wing optimization presented in this publication. In addition, the author would like to thank Lars Reimer from the DLR-institute of Aerodynamics and Flow Technology for providing Python modules to control the fluid structure coupling and the control surface deflections in the FlowSimulator environment. The author gratefully acknowledges the scientific support and HPC resources provided by the German Aerospace Center (DLR). The HPC system CARA is partially funded by "Saxon State Ministry for Economic Affairs, Labour and Transport" and "Federal Ministry for Economic Affairs and Climate Action".

6. Contact Author Email Address

tobias.wunderlich@dlr.de

7. Copyright Statement

References

[1] German Aerospace Center. *Towards zero-emission Aviation - How DLR's Aviation Research Strategy supports the European Green Deal 2050*. Cologne, Germany: German Aerospace Center (DLR), 2022.

[2] European Commision. *Sustainable and Smart Mobility Strategy*. Luxembourg, Belgium: Office for Official Publications of the European Communities, Dec. 2020.

[3] L. Prandtl. "Über Tragflügel kleinsten induzierten Widerstandes". In: *Zeitschrift für Flugtechnik und Motorluftschiffahrt* 24 (1933). Nachdruck in: Gesammelte Abhandlungen zur angewandten Mechanik, Hydro- und Aerodynamik, Springer-Verlag, Berlin, 1961, S. 556-561, pp. 305–306.

[4] R. T. Jones. *The Spanwise Distribution of Lift for Minimum Induced Drag of Wings Having a Given Lift and a Given Bending Moment*. Tech. rep. NACA Technical Note 2249. National Advisory Committee for Aeronautics, 1950.

[5] D. J. Pate and B. J. German. "Lift Distributions for Minimum Induced Drag with Generalized Bending Moment Constraints". In: *Journal of Aircraft* 50.3 (2013), pp. 936–946.

[6] M. D. Krengel and M. Hepperle. "Gust and Maneuver Load Alleviation in Conceptual Aircraft Design". In: *New Results in Numerical and Experimental Fluid Mechanics XIV*. Ed. by A. Dillmann et al. Notes on Numerical Fluid Mechanics and Multidisciplinary Design. Die Arbeiten sind zum Teil gefördert durch das Bundesministerium für Wirtschaft und Klimaschutz (BMWK) als Teil des LuFo VI-1 Projektes INTELWI (Förderkennzeichen: 20A1903L). Springer Cham, Sept. 2023, pp. 186–195.

[7] R. M. Bogenfeld et al. "Damage Tolerance Allowable Calculation for the Aircraft Design with Static Ultimate Load". In: *Composite Structures* (Dec. 2023). Ed. by N. Fantuzzi et al.

[8] J. R. R. A. Martins. "Fuel Burn Reduction Through Wing Morphing". In: *Encyclopedia of Aerospace Engineering*. John Wiley & Sons, Ltd, 2016, pp. 1–7.

[9] J. Szodruch and R. Hilbig. "Variable wing camber for transport aircraft". In: *Progress in Aerospace Sciences* 25.3 (1988), pp. 297–328.

[10] D. A. Burdette et al. "Aerostructural design optimization of a continuous morphing trailing edge aircraft for improved mission performance". In: *17th AIAA/ISSMO Multidisciplinary Analysis and Optimization Conference*.

[11] D. Reckzeh. “Multifunctional Wing Moveables: Design of the A350XWB and the Way to Future Concepts”. In: *29th Congress of the International Council of the Aeronautical Sciences, ICAS 2014*. Sept. 2014.

[12] T. F. Wunderlich and F. Siebert. “Optimization of control surface deflections on the high aspect ratio wing to improve cruise flight performance”. In: *New Results in Numerical and Experimental Fluid Mechanics XIV- Contributions to the 23rd STAB/DGLR Symposium Berlin*. Ed. by A. Dillmann et al. Cham: Springer, Nov. 2022, pp. 206–215.

[13] T. F. Wunderlich et al. “Global Aerostructural Design Optimization of More Flexible Wings for Commercial Aircraft”. In: *Journal of Aircraft* 58.6 (2021), pp. 1254–1271.

[14] M. M. Munk. *The Minimum Induced Drag of Airfoils*. Tech. rep. NACA Report 121. National Advisory Committee for Aeronautics, 1921.

[15] H. Schlichting and E. Truckenbrodt. *Aerodynamik des Flugzeuges, Zweiter Band: Aerodynamik des Tragflügels (Teil II), des Rumpfes, der Flügel-Rumpf-Anordnung und der Leitwerke*. 3. Auflage. Berlin Heidelberg: Springer, 2001.

[16] H. Schlichting and E. Truckenbrodt. *Aerodynamik des Flugzeuges, Erster Band: Grundlagen der Strömungsmechanik, Aerodynamik des Tragflügels (Teil I)*. 3. Auflage. Berlin Heidelberg: Springer, 2001.

[17] B. S. Stratford. “The prediction of separation of the turbulent boundary layer”. In: *Journal of Fluid Mechanics* 5 (1959), pp. 1–16.

[18] T. F. Wunderlich and L. Reimer. “Integrated Process Chain for Aerostructural Wing Optimization and Application to an NLF Forward Swept Composite Wing”. In: *AeroStruct: Enable and Learn How to Integrate Flexibility in Design.* Ed. by R. Heinrich. Vol. 138. Notes on Numerical Fluid Mechanics and Multidisciplinary Design (NNFM). Cham: Springer International Publishing, 2018, pp. 3–33.

[19] T. F. Wunderlich. “Multidisciplinary Optimization of Flexible Wings with Manoeuvre Load Reduction for Highly Efficient Long-Haul Airliners”. In: *Deutscher Luft- und Raumfahrtkongress 2022*. Sept. 2022.

[20] A. B. Lambe and J. R. R. A. Martins. “Extensions to the Design Structure Matrix for the Description of Multidisciplinary Design Analysis and Optimization Processes”. In: *Structural and Multidisciplinary Optimization* 46 (2012), pp. 273–284.

[21] C. M. Liersch and M. Hepperle. “A distributed toolbox for multidisciplinary preliminary aircraft design”. In: *CEAS Aeronautical Journal* 2.1–4 (2011), pp. 57–68.

[22] A. Rempke. “Netzdeformation mit Elastizitätsanalogie in multidisziplinärer FlowSimulator-Umgebung”. In: *20. DGLR - Fach - Symposium der STAB 2016*. Vol. 2016. 2016, pp. 128–129.

[23] L. Reimer et al. “Towards Higher-Precision Maneuver and Gust Loads Computations of Aircraft: Status of Related Features in the CFD-Based Multidisciplinary Simulation Environment FlowSimulator”. In: *New Results in Numerical and Experimental Fluid Mechanics XII*. Ed. by A. Dillmann et al. Cham: Springer International Publishing, 2020, pp. 597–607.

[24] T. Führer et al. “Automated model generation and sizing of aircraft structures”. In: *Aircraft Engineering and Aerospace Technology* 88.2 (2016), pp. 268–276.

[25] C. Geuzaine and J.-F. Remacle. “Gmsh: A 3-D finite element mesh generator with built-in pre- and post-processing facilities”. In: *International Journal for Numerical Methods in Engineering* 79.11 (2009), pp. 1309–1331.

[26] T. Gerhold. “Overview of the Hybrid RANS TAU-Code”. In: *MEGAFLOW - Numerical Flow Simulation for Aircraft Design*. Ed. by N. Kroll and J. K. Fassbender. Vol. 89. Berlin, Heidelberg: Springer Berlin Heidelberg, 2005, pp. 81–92.

[27] D. Schwamborn et al. “The DLR TAU-Code: Recent Applications in Research and Industry”. In: *European Conference on Computational Fluid Dynamics, ECCOMAS CFD 2006 Conference, Delft, The Netherlands*. 2006.

[28] M. Meinel and G. O. Einarsson. “The FlowSimulator framework for massively parallel CFD applications”. In: *PARA 2010 conference, 6-9 June, Reykjavik, Iceland*. 2010.

[29] E. N. Tinoco et al. “Summary Data from the Sixth AIAA CFD Drag Prediction Workshop: CRM Cases”. In: *Journal of Aircraft* 55.4 (2018), pp. 1352–1379.

[30] S. Dähne et al. “Steps to Feasibility for Laminar Wing Design in a Multidisciplinary Environment”. In: *29th Congress of the International Council of the Aeronautical Sciences, ICAS 2014*. Sept. 2014.

[31] H. Barnewitz and B. Stickan. “Improved Mesh Deformation”. In: *Management and Minimisation of Uncertainties and Errors in Numerical Aerodynamics: Results of the German collaborative project MUNA*. Ed. by B. Eisfeld et al. Vol. 122. Berlin, Heidelberg, 2013, pp. 219–243.

[32] G. A. Wilke. “Variable-Fidelity Methodology for the Aerodynamic Optimization of Helicopter Rotors”. In: *AIAA Journal* 57.8 (2019), pp. 3145–3158.

[33] D. R. Jones et al. “Efficient Global Optimization of Expensive Black-Box Functions”. In: *Journal of Global Optimization* 13.4 (1998), pp. 455–492.

[34] A. Forrester et al. *Engineering Design via Surrogate Modelling: A Practical Guide*. Wiley, 2008.

[35] L. Ju et al. “Probabilistic methods for centroidal Voronoi tessellations and their parallel implementations”. In: *Parallel Computing* 28.10 (2002), pp. 1477–1500.

[36] D. G. Krige. “A Statistical Approach to Some Basic Mine Valuation Problems on the Witwatersrand”. In: *Journal of the Chemical, Metallurgical and Mining Society of South Africa* 52.6 (Dec. 1951), pp. 119–139.

[37] R. Storn and K. Price. “Differential Evolution - A Simple and Efficient Heuristic for global Optimization over Continuous Spaces”. In: *Journal of Global Optimization* 11.4 (1997), pp. 341–359.

[38] J. A. Nelder and R. Mead. “A Simplex Method for Function Minimization”. In: *Computer Journal* 7 (1965), pp. 308–313.

[39] N. E. Antoine and I. M. Kroo. “Aircraft Optimization for Minimal Environmental Impact”. In: *Journal of Aircraft* 41.4 (2004), pp. 790–797.